Supplementary Information

Molybdate-Mediated Self-Healing NiMoFeO/Ni Electrodes for Durable Alkaline OER

Zude Shen[#], Ang Li[#], Min Deng, Jiangbin Han, Hongmei Chen* and Ling Zhang*

Center of Advanced Electrochemical Energy, State Key Laboratory of Advanced Chemical Power Sources, College of Chemistry and Chemical Engineering, Chongqing University, Chongqing, 400044 P.R. China

*Corresponding author. Email: chenhongmei926@163.com; zhanglinggood@cqu.edu.cn

1. Experimental section

1.1 Materials

All chemicals were used as received unless otherwise specified. Hydrochloric acid, nitric acid, sulfuric acid, nickel nitrate hexahydrate, sodium molybdate dihydrate, potassium ferricyanide, potassium hydroxide, absolute ethanol, acetone, and urea were purchased from Chongqing Chuandong Chemical Co., Ltd. Ni foam was purchased from Tianjin Anuohe New Energy Technology Co., Ltd. RuO_2 was purchased from Aladdin. Pt/C with a Pt loading of 20 wt% was obtained from Johnson Matthey. Nafion solution was purchased from DuPont. Ultrapure water was obtained from an in-house ultrapure water system.

1.2 Preparation process

Pretreatment of the Ni foam substrate

Before synthesis, Ni foam (50 × 10 × 1.5 mm) was pretreated to remove surface oxides and organic contaminants. The Ni foam was sonicated in a mixture of ethanol and acetone (1:1, v/v) for 20 min, followed by sonication in 3 M HCl for another 20 min. It was then thoroughly rinsed with ultrapure water until the rinse solution became neutral and dried before use.

Preparation of reference electrodes for HER and OER

The reference electrodes were prepared as follows. RuO_2 (for OER) or Pt/C (for HER) was dispersed in 50 μL of 0.5 wt% Nafion solution and 450 μL of anhydrous ethanol, followed by sonication for 30 min to form a homogeneous ink. The ink was drop-cast onto a 1 cm^2 piece of pretreated Ni foam and dried under ambient conditions. The catalyst loading was fixed at 1.0 mg cm^{-2} for both RuO_2/Ni and Pt/C/Ni.

Preparation of NiO/Ni, NiFeO/Ni, NiMoO/Ni, and NiMoFeO/Ni electrodes

NiO/Ni and NiFeO/Ni were prepared from a hydrothermally synthesized $Ni(OH)_2$/Ni precursor. Briefly, $Ni(NO_3)_2 \cdot 6H_2O$ (1.222 g) and urea (1.297 g) were dissolved in 70 mL of ethanol/H_2O (v/v = 6:1), and the resulting solution was transferred into a Teflon-lined stainless-steel autoclave containing pretreated Ni foam. The hydrothermal reaction was carried out at 120 °C for 6 h. After cooling to room temperature, the resulting precursor electrode was thoroughly washed with deionized water and dried at 60 °C for 6 h. NiO/Ni was obtained by directly annealing the precursor at 450 °C for 2 h under flowing N_2 (50 sccm) at a heating rate of 5 °C min^{-1}. NiFeO/Ni was prepared by first subjecting the precursor to ion exchange in 50 mL of 15 mM $K_3Fe(CN)_6$

solution at 80 °C for 15 min, followed by annealing under the same conditions.

NiMoO/Ni and NiMoFeO/Ni were prepared in a similar manner using a hydrothermally synthesized $NiMoO_4$/Ni precursor. Specifically, $Ni(NO_3)_2 \cdot 6H_2O$ (0.233 g) and $Na_2MoO_4 \cdot 2H_2O$ (0.193 g) were dissolved in 70 mL of ethanol/H_2O (v/v = 6:1), and the resulting solution was transferred into a Teflon-lined stainless steel autoclave containing pretreated Ni foam. The hydrothermal reaction was carried out at 160 °C for 8 h. After cooling to room temperature, the resulting precursor electrode was thoroughly washed with deionized water and vacuum-dried at 60 °C for 6 h. NiMoO/Ni was obtained by directly annealing the precursor at 450 °C for 2 h under flowing N_2 (50 sccm) with a heating rate of 5 °C min^{-1}. NiMoFeO/Ni was prepared by subjecting the precursor to ion exchange in 50 mL of $K_3Fe(CN)_6$ solution at 80 °C for 15 min prior to annealing under the same conditions. $K_3Fe(CN)_6$ solutions with concentrations of 5, 10, 15, 20, and 25 mM were used for the ion-exchange step. The corresponding products are denoted as NiMoFeO/Ni-x, where x represents the concentration of $K_3Fe(CN)_6$ used during the ion-exchange process. Unless otherwise specified, the sample prepared using 15 mM $K_3Fe(CN)_6$ is denoted as NiMoFeO/Ni.

1.3 Characterization methods

Material characterization

Powder X-ray diffraction (XRD) patterns were collected on an X'Pert PRO MPD diffractometer. Scanning electron microscopy (SEM) images were acquired on an FEI Nova 400 microscope, and transmission electron microscopy (TEM) images were collected on an FEI Tecnai F20 microscope. X-ray photoelectron spectroscopy (XPS) measurements were carried out on a Thermo ESCALAB 250Xi spectrometer equipped with an Al Kα X-ray source. The binding energies were calibrated with reference to adventitious carbon at 284.8 eV. Raman spectra were recorded using a laser excitation wavelength of 512 nm. Inductively coupled plasma optical emission spectroscopy (ICP-OES) measurements were performed on a Thermo Scientific iCAP 6300 Duo instrument.

Electrochemical measurements

All OER measurements were carried out in a standard three-electrode configuration using a Metrohm Autolab 72703 electrochemical workstation. Overall water splitting was evaluated in a two-electrode cell using the same workstation. The catalyst-coated electrode served as the working electrode, a graphite sheet was used as the counter electrode, and a Hg/HgO electrode was used as

the reference electrode. All measured potentials were converted to the reversible hydrogen electrode scale according to the equation $E_{RHE} = E_{Hg/HgO} + 0.098 + 0.059\times$ pH. All polarization curves were corrected for iR drop according to $E_{corrected} = E_{measured} - iR_s$, where R_s was obtained from electrochemical impedance spectroscopy. 1.0 M KOH was used as the electrolyte for OER.

In the three-electrode measurements, linear sweep voltammetry was performed at a scan rate of 2 mV s^{-1}. The potential range was 1.0 - 1.8 V vs. RHE for low current density OER measurements and 1.0 - 2.0 V vs. RHE for high current density OER measurements above 500 mA cm^{-2}. For overall water splitting, the cell voltage range was 1.0 - 2.5 V.

For double-layer capacitance measurements, cyclic voltammetry (CV) was conducted at different scan rates within the non-Faradaic region. The average capacitive current at a fixed potential was plotted against the scan rate, and the slope of the linear fit was taken as the double layer capacitance (C_{dl}). The electrochemically active surface area was estimated from ECSA = C_{dl}/C_s using a specific capacitance of 40 μF cm^{-2}.

Electrochemical impedance spectroscopy was carried out over a frequency range from 10 kHz to 0.01 Hz with an amplitude of 10 mV at a bias potential of 1.48 V vs. RHE. Chronopotentiometry was performed at a constant current density, and the electrode potential in the three-electrode OER test or the cell voltage in the two-electrode water-splitting test was recorded as a function of time.

2. Supplementary notes

2.1 Optimization of Fe incorporation in NiMoFeO/Ni

The OER performance of NiMoFeO/Ni could be tuned by varying the concentration of $K_3Fe(CN)_6$ during synthesis. The activity improved with increasing $K_3Fe(CN)_6$ concentration and reached an optimum at 15 mM. The optimized sample, denoted as NiMoFeO/Ni-15, delivered overpotentials of 221 and 313 mV at 10 and 500 mA cm^{-2}, respectively (Fig. S5a), and showed the smallest Tafel slope of 50.73 mV dec^{-1} (Fig. S5b). The slight difference from the Tafel slope in the comparative OER test arises from independent measurements on separately prepared electrodes. Electrochemical impedance spectroscopy and double-layer capacitance measurements further showed that NiMoFeO/Ni-15 had the lowest charge-transfer resistance and the largest electrochemically active surface area, with a C_{dl} value of 122.28 mF cm^{-2} (Fig. S5c, d). After normalization to the ECSA, this sample still showed the highest ECSA-normalized activity (Fig. S6). Therefore, NiMoFeO/Ni-15 was selected for detailed investigation and is hereafter referred to as NiMoFeO/Ni.

2.2 Molybdate redeposition and interfacial maintenance

The time-dependent ICP-OES, XPS and Raman results indicate that molybdate is not irreversibly lost during OER, but undergoes partial redeposition on the reconstructed electrode surface. The possible redeposition process can be rationalized by interfacial enrichment of MoO_4^{2-} near the anodically polarized electrode, followed by interaction with hydroxylated/oxo NiFeOOH surface sites. Similar molybdate dissolution/re-adsorption behavior has been reported in related NiFe-based OER systems, where dissolved MoO_4^{2-} can be re-adsorbed to modulate the local structure/electronic environment.[1, 2] Therefore, the recovered Mo 3d signal and the weak reappearance of Mo–Ni–O/O–Mo–O Raman features in this work are assigned mainly to interfacial redeposition/complexation. However, because the present data do not directly resolve the atomic position of Mo, possible near-surface incorporation cannot be fully excluded.

The present results do not prove that redeposited Mo acts as an independent redox-active OER center. Instead, redeposited Mo is more reasonably considered as an interfacial promoter that stabilizes and modulates the reconstructed NiFeOOH surface. This interpretation is supported by the increased Ni^{3+} fraction after MoO_4^{2-} replenishment, the reduced charge-transfer resistance and the recovered OER activity. It is also consistent with recent reports showing that Mo-related species

in NiFe oxyhydroxides can induce Ni–Fe–Mo electronic interactions and improve alkaline OER activity. [1] Therefore, the catalytic function of redeposited Mo is described as stabilization/electronic modulation of NiFeOOH rather than a directly proven Mo-centered catalytic cycle.

2.3 Concentration-dependent molybdate effect

As shown in Fig. S12, the OER performance of NiFeO/Ni depends strongly on the concentration of added MoO_4^{2-}. The activity reaches an optimum at 0.05 M MoO_4^{2-}, while further increasing the concentration to 0.1 M leads to decreased performance. This trend suggests that molybdate plays an interfacial regulatory role rather than simply increasing electrolyte conductivity. A low MoO_4^{2-} concentration may be insufficient to maintain the reconstructed surface, whereas excessive MoO_4^{2-} may partially block active sites or disturb interfacial charge transfer. The correlation between electrolyte MoO_4^{2-} concentration, XPS-derived surface Mo content and OER metrics is summarized in Table S3. The surface Mo content increases with electrolyte MoO_4^{2-} concentration, whereas the OER activity follows an optimum at 0.05 M MoO_4^{2-}, suggesting that moderate interfacial molybdate is beneficial while excessive molybdate may hinder active-site exposure or interfacial charge transfer.

The electrolyte-refreshing experiment in Fig. S14 further supports this interpretation. Replacing the used electrolyte with fresh KOH does not recover the OER activity, whereas adding 0.05 M MoO_4^{2-} to the refreshed electrolyte restores the activity and improves charge-transfer kinetics. These results indicate that an appropriate molybdate reservoir in the electrolyte is beneficial for maintaining the reconstructed active interface. Although the MoO_4^{2-}-conditioned NiFeO/Ni control shows improved low-current activity, NiMoFeO/Ni still delivers a lower overpotential at 500 mA cm^{-2} and much longer high-current durability. Therefore, this control experiment is used to isolate the interfacial regulatory role of molybdate rather than to replace the integrated NiMoFeO/Ni electrode.

2.4 Surface-limited reconstruction

The reconstruction depth cannot be quantified from the present data. XPS and Raman spectroscopy mainly probe the surface or near-surface region; therefore, the formation of NiFeOOH is assigned primarily to the electrolyte-accessible outer region of the nanosheets. The largely retained nanosheet morphology after OER, as observed by post-OER SEM (Fig. S16), suggests that the bulk scaffold is not completely destroyed during reconstruction. Further depth-profiling XPS,

cross-sectional STEM/EELS or operando X-ray absorption spectroscopy would be required to determine the exact reconstruction thickness.

2.5 Practical implication of molybdate supplementation

The present results do not imply that continuous high-concentration molybdate feeding is required for practical alkaline electrolysers. In a closed or recirculating electrolyte, molybdate released from the catalyst may establish a local dissolution/redeposition equilibrium. However, electrolyte refreshing or prolonged high-current operation may reduce the available molybdate reservoir and weaken the interfacial maintenance effect. Therefore, low-level molybdate conditioning or periodic replenishment may be considered for sustaining reconstructed NiFeOOH interfaces, while additive concentration, membrane compatibility, crossover, cost and long-term accumulation should be further evaluated before practical application.

3. Material characterization and electrochemical data

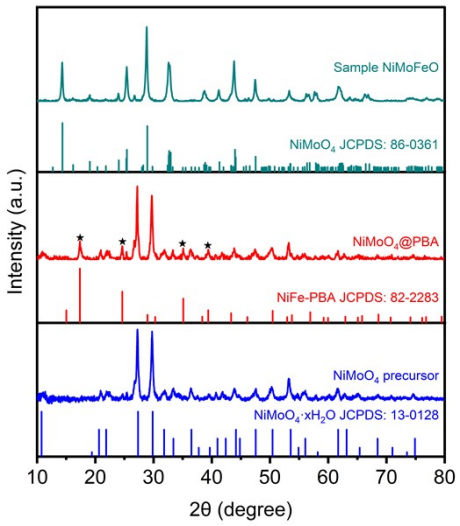

Figure S1. PXRD patterns of $NiMoO_4$ precursor, $NiMoO_4$@PBA and NiMoFeO.

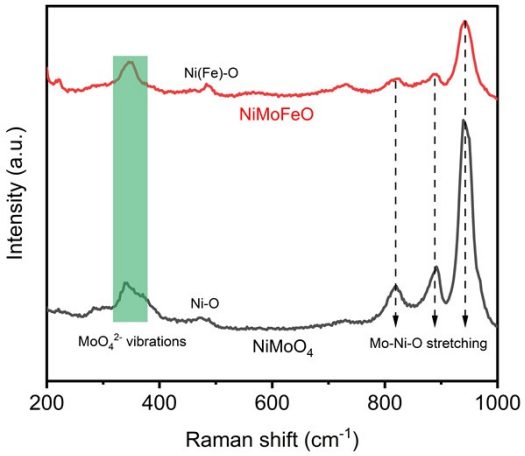

Figure S2. Raman spectra of $NiMoO_4$/Ni and NiMoFeO/Ni.

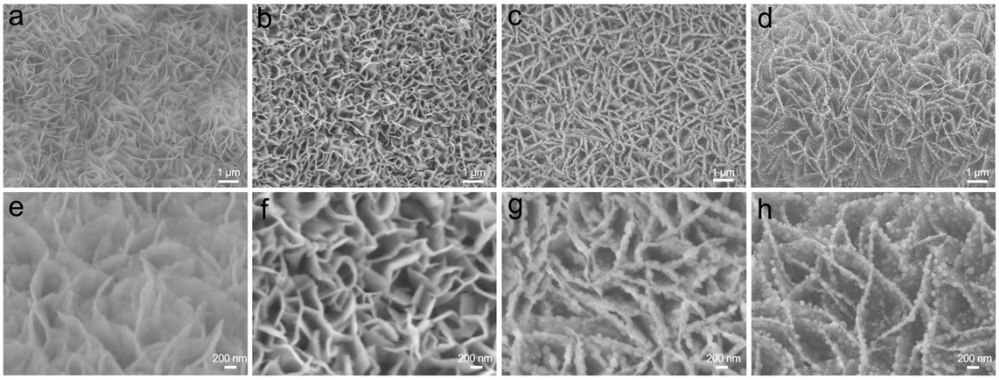

Figure S3. SEM images of different electrodes: (a) NiO/Ni, (b) NiMoO/Ni, (c) NiFeO/Ni and (d) NiMoFeO/Ni.

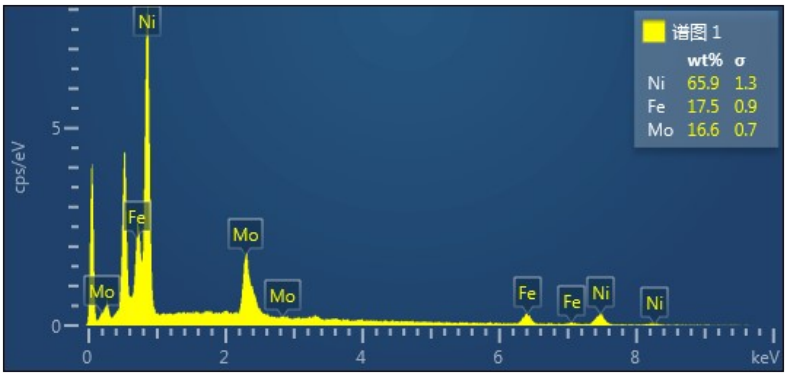

Figure S4. EDS spectrum of the NiMoFeO/Ni electrode.

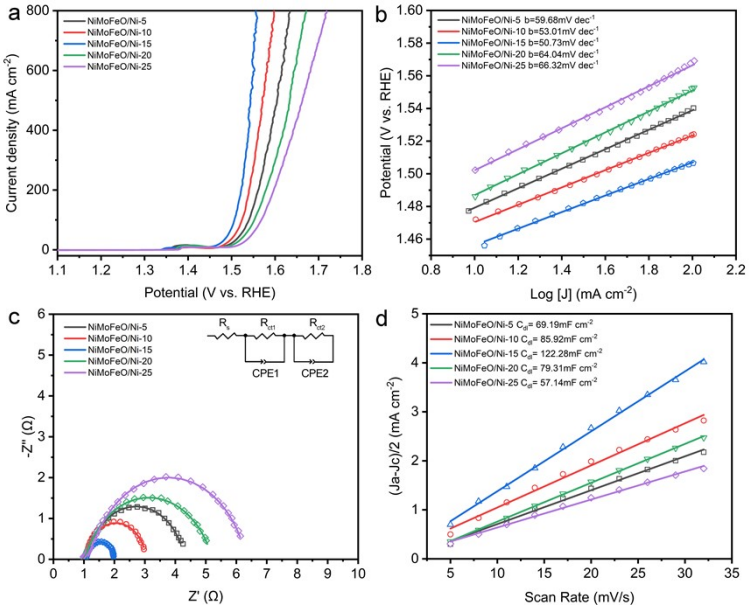

Figure S5. OER performance of NiMoFeO/Ni electrodes prepared using different $K_3Fe(CN)_6$ concentrations: (a) LSV curves, (b) corresponding Tafel slopes, (c) EIS Nyquist plots, and (d) C_{dl} values.

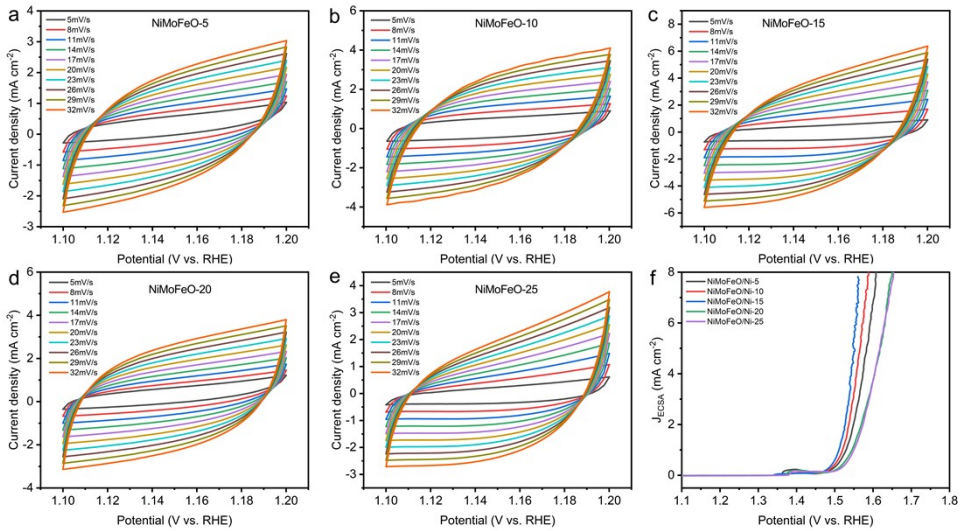

Figure S6. CV curves collected in the non-Faradaic region at different scan rates for NiMoFeO/Ni prepared using different $K_3Fe(CN)_6$ concentrations: (a) 5 mM, (b) 10 mM, (c) 15 mM, (d) 20 mM, (e) 25 mM, and (f) ECSA-normalized LSV curves.

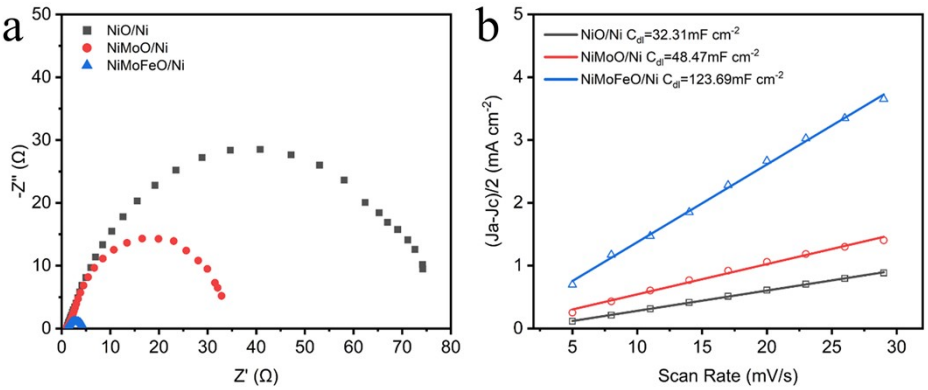

Figure S7. OER performance of different electrodes (NiMoFeO/Ni, NiO/Ni, NiMoO/Ni and RuO_2/Ni): (a) EIS, (b) Cdl values.

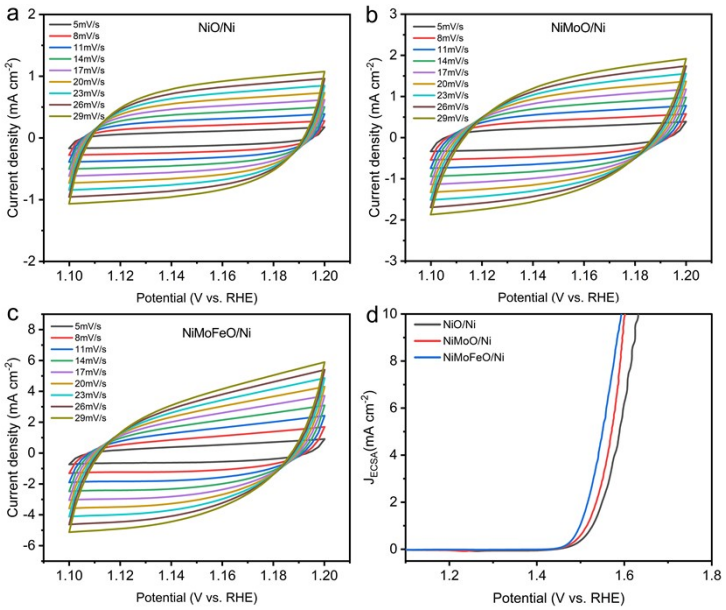

Figure S8. CV curves collected in the non-Faradaic region at different scan rates: (a) NiO/Ni, (b) NiMoO/Ni, (c) NiMoFeO/Ni, and (d) the corresponding ECSA-normalized LSV curves.

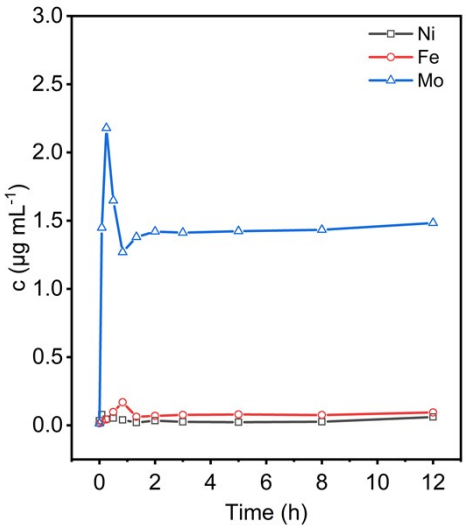

Figure S9. Time-dependent concentrations of Ni, Mo, and Fe in the electrolyte quantified by ICP-OES during OER at 100 mA cm^{-2}.

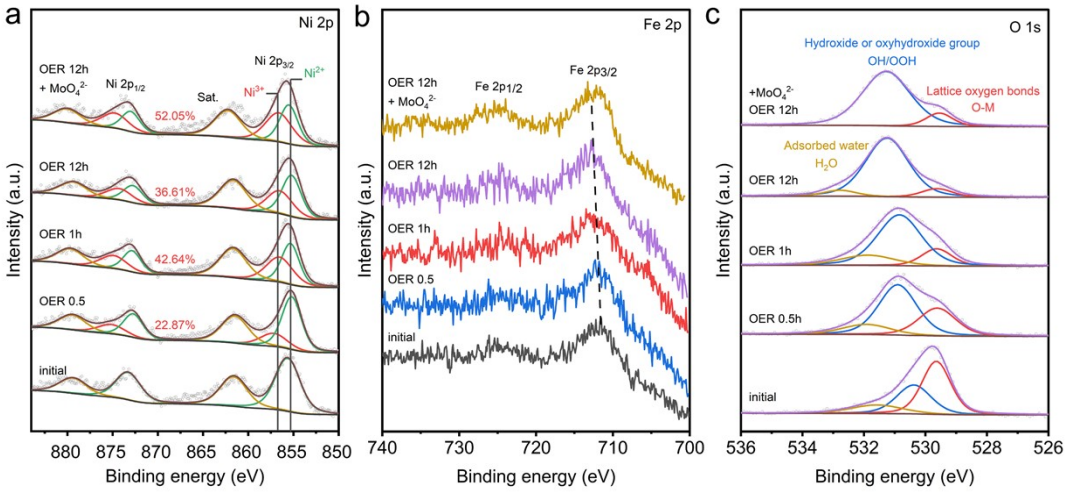

Figure S10. High-resolution Ni 2p Fe 2p and O 1s XPS spectra of NiMoFeO/Ni after OER for 0.5, 1, and 12 h in KOH, as well as after 12 h in KOH containing 0.05 M MoO_4^{2-}.

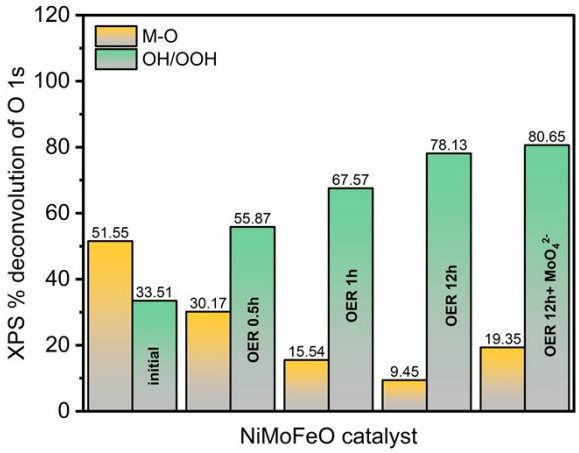

Figure S11. Relative contents of M-O and OH/OOH species on the NiMoFeO/Ni electrode.

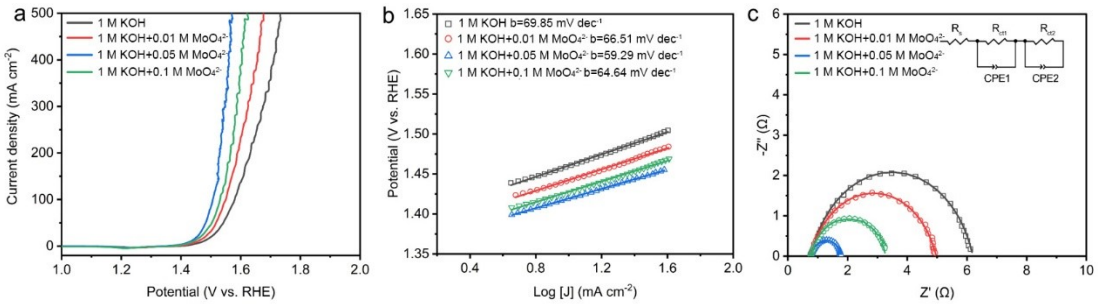

Figure S12. OER performance of NiFeO/Ni in MoO_4^{2-}-containing electrolytes with different concentrations: (a) LSV curves, (b) corresponding Tafel plots, and (c) EIS Nyquist plots.

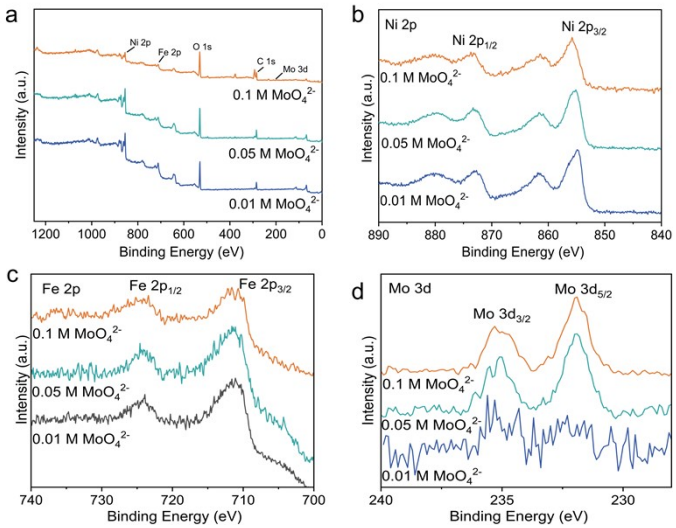

Figure S13. XPS results of NiFeO/Ni electrodes after reaction tests with different concentrations of added MoO_4^{2-}. (a) Survey spectra; (b–d) High-resolution X-ray photoelectron spectra of Ni 2p, Fe 2p and Mo 3d.

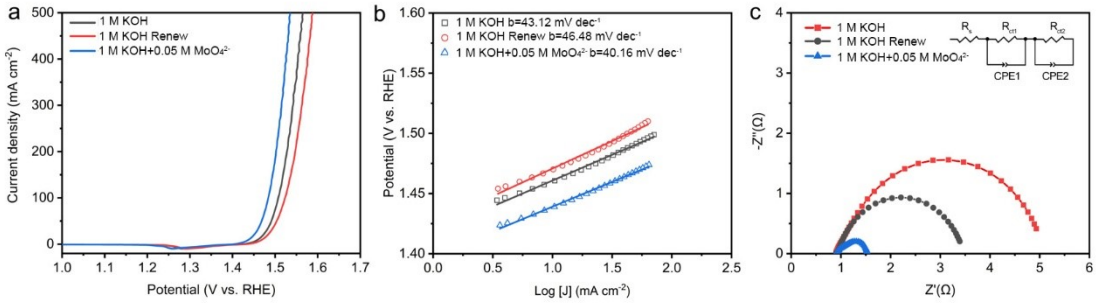

Figure S14. OER performance of NiMoFeO/Ni in the initial KOH, refreshed KOH, and refreshed KOH containing molybdate: (a) polarization curves, (b) corresponding Tafel plots, and (c) EIS Nyquist plots.

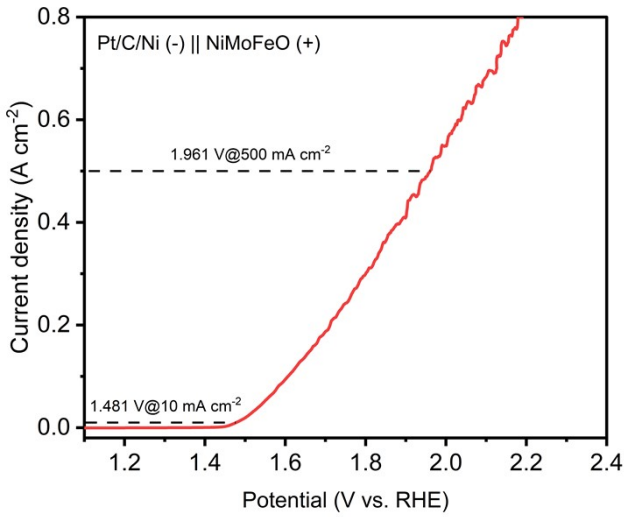

Figure S15. Overall water splitting performance of a two-electrode cell using Pt/C/Ni as the cathode and NiMoFeO/Ni as the anode: LSV curves.

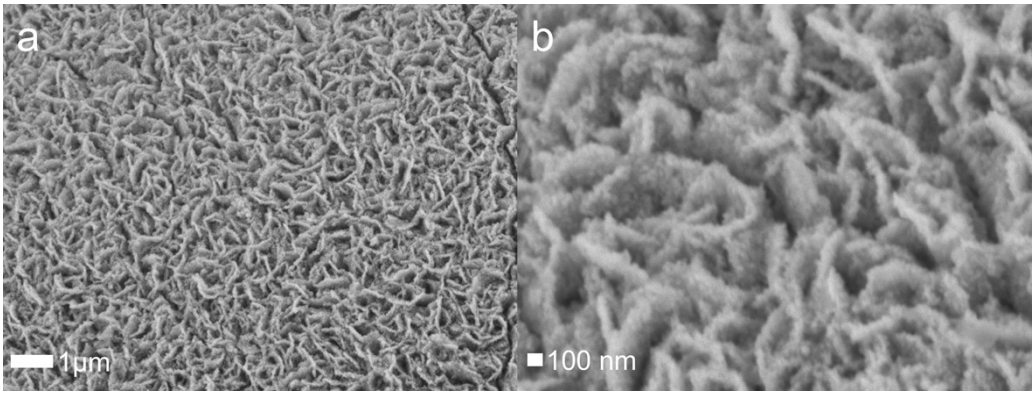

Figure S16. SEM images of NiMoFeO/Ni electrodes after OER testing.

Table S1. ICP-OES analysis of the NiMoFeO/Ni electrode.

Elements	Ni	Mo	Fe
Wt.%	67.61	15.30	17.09
At.%	71.22	9.86	18.92

Table S2. Brief comparison with representative NiFe-based OER catalysts operated at high current densities.

Catalyst	Electrolyte	Overpotentials	Tafel slope (mV dec^{-1})	Durability	Reference
NiMoFeO/Ni	1.0 M KOH	η_{10} = 221 mV; η_{500} = 313 mV	44.5	300 h @ 500 mA cm^{-2}; $\Delta\eta$ = 58 mV	**This work**
CeO_2-$NiFeO_xH_y$	1.0 M KOH	η_{10} = 214 mV; η_{500} = 659 mV	72.46	210 h @ 500 mA cm^{-2}	3
NFM30-N	1.0 M KOH	η_{100} = 282 mV; η_{500} = 323 mV	44.1	100 h @ 500 mA cm^{-2}	4
CeF_3-NiFeLDH	1.0 M KOH	η_{20} = 180 mV; η_{1000} = 340 mV	51	90 h @ 500 mA cm^{-2}	5
NiFe-LDH-4	1.0 M KOH	η_{10} = 175 mV; η_{50} = 235 mV; η_{500} = 354 mV	90.32	50 h @ 500 mA cm^{-2}	6
NiFeCo-0.6	1.0 M KOH	η_{100} = 261 mV; η_{500} = 318 mV; η_{1000} = 353 mV	38	300 h @ 500 mA cm^{-2}	7
O–NiFe-LDH@NF	1.0 M KOH	η_{10} = 197 mV; η_{500} = 354 mV	50.1	300 h @ 500 mA cm^{-2}	8
C-NFF-LDH/Fe_2O_3	1.0 M KOH	η_{10} = 220 mV; η_{50} = 248 mV	31.2	100 h @ 500 mA cm^{-2}	9
Cr-doped (4 mol%) $FeNi_3$/$NiFe_2O_4$	1.0 M KOH	η_{100} = 292 mV; η_{300} = 330 mV; η500 = 360 mV	55	200 h @ 1000 mA cm^{-2}	10
Fe-NiWB/PW	1.0 M KOH	η_{10} = 248 mV; η_{500} = 350 mV; η_{1000} = 363 mV	42.59	2000 h @ 500 mA cm^{-2}	11
NFMN-FeOOH	1.0 M KOH	η_{10} = 256 mV; η_{500} = 308 mV	36	300 h @ 500 mA cm^{-2}	12
FeNiZn/$FeNi_3$@NiFe	1.0 M KOH	η_{50} = 244 mV; η_{100} = 258 mV; η_{500} = 315 mV	44.7	400 h @ 500 mA cm^{-2}	13
NiFe-LDH/$CoMoO_4$/NF	1.0 M KOH	η_{100} = 280 mV; η_{300} = 334 mV; η_{500} = 360 mV	58.2	100 h @ 500 mA cm^{-2}	14
NiFe/$NiFe_2O_4$	1.0 M KOH	η_{10} = 146 mV; η_{100} = 212 mV	24.11	>100 h @ 500 mA cm^{-2}	15

Note: The values are taken as reported in the cited literature. Differences in catalyst loading, electrode configuration, iR correction, electrolyte purification and testing protocols should be considered when comparing OER performance.

Table S3. Correlation between electrolyte MoO_4^{2-} concentration and OER metrics of NiFeO/Ni.

MoO_4^{2-} concentration in 1.0 M KOH	Mo/(Ni+Fe+Mo) from XPS (at%)	η_{10} (mV)	η_{500} (mV)	Tafel slope (mV dec^{-1})	Rct (Ω)
0 M	0	244	500	69.85	5.3
0.01 M	1.07	229	440	66.51	4.2
0.05 M	3.60	200	340	59.29	0.9
0.1 M	6.03	210	390	64.64	2.5

Reference

1. Y. Qiao, Y. Pan, W. Fan, G. Long and F. Zhang, *Chem. Commun.*, 2024, **60**, 11287-11290.
2. J. Zhou, L. Liu, H. Ren, L. Li, W. Song, N. Li, X. Shi, C. Kou, Y. Sun, M. Han, H. Wang, J. Han, K. Liu, C. D. Momo Jr., Y. Liu, D. Feng, W. Zhu, S. Chen, H. Jiang, Y. Liu and H. Liang, *Inorg. Chem. Front.*, 2024, **11**, 498-507.
3. L. Li, L. Qiao, D. Liu, Z. Yu, K. An, J. Yang, C. Liu, Y. Cao and H. Pan, *Small*, 2025, **21**, 2403992.
4. W. Zhang, L. Hou, J. Wang, Z. Long, X. Lu, X. Yu and X. Li, *J. Mater. Sci. Technol.*, 2025, **211**, 11-21.
5. R. Kaur, A. Gaur, V. Pundir, K. Arun and V. Bagchi, *J. Colloid Interface Sci.*, 2024, **672**, 736-743.
6. X. Li, S.-l. Xu, J. Li, S.-s. Zhang, B.-y. Zhang, R.-d. Zhao, D.-p. Zhao and F.-f. Wu, *Nanoscale Adv.*, 2025, **7**, 5546-5560.
7. Y. Wu, Y. Li, Z. Xie, Y. Wang, Y. Wang and B. Wei, *Chem. Eng. J.*, 2024, **488**, 151086.
8. Z. Gong, X. Wang, W. Pi, N. Yao, Z. Fang, H. Bao and Q. Wu, *Mater. Today Phys.*, 2024, **43**, 101399.
9. Y. Zhou, J. Gao, M. Ju, Y. Chen, H. Yuan, S. Li, J. Li, D. Guo, M. Hong and S. Yang, *ACS Appl. Mater. Interfaces*, 2024, **16**, 28526-28536.
10. S. Khatun, S. Pal and P. Roy, *J. Alloys Compd.*, 2024, **977**, 173393.
11. Y. Liao, L. Li, J. Zhang, Y. Chen, S. Luo, Y. Qing, C. Tian, G. He and Y. Wu, *Adv. Mater.*, 2026, **38**, 2516751.
12. H. Du, T. Wang, S. He, B. Li, K. Wang, Q. Chen, Z. Du, W. Ai and W. Huang, *Adv. Funct. Mater.*, 2024, **34**, 2311854.
13. Q. Zhou, C. Xu, J. Hou, W. Ma, T. Jian, S. Yan and H. Liu, *Nano-Micro Lett.*, 2023, **15**, 95.
14. X. Xiao, R. Ma, K. Jiang, L. Ma, Q. Wang, S. Meng, T. Yang, Z. Qiu, R. Hu and L. Huang, *Fuel*, 2025, **379**, 132978.
15. D. Fang, G. Yang, Y. Fu, D. Gao, X. Wang, Y. Mao and J. Li, *Chem. Commun.*, 2025, **61**, 19261-19264.